Monthly Notices
of the
ROYAL ASTRONOMICAL SOCIETY

Mon. Not. R. Astron. Soc. **400,** 670–676 (2009) doi:10.1111/j.1365-2966.2009.15517.x

A search for neutral carbon towards two $z = 4.05$ submillimetre galaxies, GN 20 and GN 20.2

C. M. Casey,[1⋆] S. C. Chapman,[1] E. Daddi,[2] H. Dannerbauer,[3] A. Pope,[4] D. Scott,[5] F. Bertoldi,[6] R. J. Beswick,[7] A. W. Blain,[8] P. Cox,[9] R. Genzel,[10] T. R. Greve,[3] R. J. Ivison,[11,12] T. W. B. Muxlow,[7] R. Neri,[9] A. Omont,[13] I. Smail[14] and L. J. Tacconi[10]

[1]*Institute of Astronomy, Madingley Road, Cambridge CB3 0HA*
[2]*Laboratoire AIM, CEA/DSM-CNRS-Université Paris Diderot, Irfu/SAp, Orme des Merisiers, F-91191 Gif-sur-Yvette, France*
[3]*MPIA, Königstuhl 17, D-69117 Heidelberg, Germany*
[4]*NOAO, 950 North Cherry Ave, Tucson, AZ 85719, USA*
[5]*Department of Physics and Astronomy, University of British Columbia, Vancouver, BC V6T 1Z1, Canada*
[6]*Argenlander Institute for Astronomy, University of Bonn, Auf dem Hügel 71, 53121 Bonn, Germany*
[7]*Jodrell Bank Centre for Astrophysics, School of Physics and Astronomy, University of Manchester, Oxford Road, Manchester M13 9PL*
[8]*Department of Astronomy, California Institute of Technology, 1200 E California Blvd, Pasadena, CA 91125, USA*
[9]*Institut de Radio Astronomie Millimetrique (IRAM), 38406 St. Martin d'Heres, France*
[10]*MPE, Giessenbachstrasse 1, D-85741 Garching, Germany*
[11]*UK Astronomy Technology Centre, Royal Observatory, Blackford Hill, Edinburgh EH9 3HJ*
[12]*Institute for Astronomy, University of Edinburgh, Blackford Hill, Edinburgh EH9 3HJ*
[13]*Institut d'Astrophysique de Paris, CNRS and Université Pierre et Marie Curie, 98 Bis Boulevard Arago, 75014 Paris, France*
[14]*Institute for Computational Cosmology, Durham University, South Road, Durham DH1 3LE*

Accepted 2009 August 7. Received 2009 August 6; in original form 2009 June 30

ABSTRACT

Using the IRAM Plateau de Bure Interferometer (PdBI) we have searched for the upper fine structure line of neutral carbon [C I($^3P_2 \rightarrow {}^3P_1$), $\nu_{\rm rest} = 809$ GHz] and ^{12}CO($J = 7 \rightarrow 6$) ($\nu_{\rm rest} = 806$ GHz) towards the submillimetre galaxies (SMGs) GN 20 (SMM J123711.9+622212, $z = 4.055$) and GN 20.2 (SMM J123708.8+622202, $z = 4.051$). The far-infrared continuum is detected at 8σ significance in GN 20, with a flux density of $S_{1.8\,\rm mm} = 1.9 \pm 0.2$ mJy, while no continuum is detected in GN 20.2. Both sources are statistically undetected in both C I($^3P_2 \rightarrow {}^3P_1$) and ^{12}CO($J = 7 \rightarrow 6$) lines; we derive line luminosity limits for both C I and CO of $L' \lesssim 2 \times 10^{10}$ K km s^{-1} pc^2. Assuming carbon excitation temperatures of $T_{\rm ex} = 30$ K (the galaxies' measured dust temperatures), we infer C I mass limits of $M_{\rm C\,I} < 5.4 \times 10^6\,{\rm M}_\odot$ (GN 20) and $M_{\rm C\,I} < 6.8 \times 10^6\,{\rm M}_\odot$ (GN 20.2). The derived C I abundance limits are $<1.8 \times 10^{-5}$ for GN 20 and $<3.8 \times 10^{-5}$ for GN 20.2, implying that the systems have Milky Way level carbon enrichment (X[C I]/X[H$_2$]) or lower, similar to high-redshift carbon-detected systems (at 5×10^{-5}) but about 50 times less than the carbon enrichment of local starburst galaxies. Observations of GN 20 and GN 20.2 in high-resolution MERLIN+VLA (Multi-Element Radio Linked Interferometer Network+Very Large Array) radio maps of GOODS-N (Great Observatories Origin Deep Survey-North) are used to further constrain the sizes and locations of active regions. We conclude that the physical gas properties of young rapidly evolving systems like GN 20 and GN 20.2 are likely significantly different than starburst/ULIRG (ultraluminous infrared galaxy) environments in the local Universe yet similar to $z \sim 2$ SMGs. Unless gravitationally amplified examples can be found, observations of galaxies like GN 20 will require the order of magnitude increase in sensitivity of the Atacama Large Millimetre Array (ALMA) to constrain their C I and high-J CO content, despite the fact that they are the brightest systems at $z \sim 4$.

Key words: galaxies: evolution – galaxies: high-redshift – galaxies: individual: GN 20 – galaxies: individual: GN 20.2 – galaxies: starburst.

⋆E-mail: ccasey@ast.cam.ac.uk

1 INTRODUCTION

Examining the molecular gas content of distant galaxies is fundamental to our understanding of galaxy formation and evolution theories. Recent observations have shown that many distant objects contain giant molecular gas reservoirs ($>10^{10}\,M_\odot$; for a review see Solomon & Vanden Bout 2005). These gas repositories are thought to provide the fuel needed to power the extreme starbursts observed at high redshift through their far-infrared (FIR) luminosities, $L_{\rm FIR} \sim 10^{12-13}\,L_\odot$ (e.g. Frayer et al. 1999; Neri et al. 2003; Greve et al. 2005; Tacconi et al. 2006; Chapman et al. 2008). In addition, detection of active galactic nucleus (AGN) in molecular gas suggests a link between the most massive starbursts, the growth of massive black holes and the onset of strong nuclear activity (Coppin et al. 2008). Molecular gas has already been detected in about 60 high-redshift sources, from star-forming galaxies to quasars, at redshifts $2 < z < 6.4$ (Bertoldi et al. 2003; Walter et al. 2003; Greve et al. 2005; Tacconi et al. 2006, 2008).

Carbon monoxide has bright rotational transitions and is therefore the most commonly observed tracer of molecular gas; however, CO lines are usually optically thick and difficult to model (e.g. Narayanan et al. 2009). In contrast, observations of optically thin neutral carbon (C I) can be used to derive gas physical properties without requiring detailed radiative transfer models. This is because carbon has a 3P fine structure forming a simple, easily analysed three-level system. The gas excitation temperature, neutral carbon column density and mass may be derived independent of any other information provided there are detections of *both* carbon lines, C I($^3P_1 \rightarrow {}^3P_0$) (492 GHz) and C I($^3P_2 \rightarrow {}^3P_1$) (809 GHz) (e.g. Stutzki et al. 1997; Weiss et al. 2003, 2005). Furthermore, observations of either C I line could potentially be used as a probe of internal gas distribution which is independent from the more luminous optically thick CO observations.

While the Earth's atmosphere has very low transmission at the rest frequency of C I($^3P_1 \rightarrow {}^3P_0$) and is virtually opaque at C I($^3P_2 \rightarrow {}^3P_1$), some studies of neutral carbon have been performed in nearby sources where the lines are bright enough to be observed. These include the Galactic Centre, molecular clouds in the galactic disc, M82 and other nearby galaxies (e.g. White et al. 1994; Stutzki et al. 1997; Gerin & Phillips 2000; Ojha et al. 2001; Israel & Baas 2002; Schneider et al. 2003; Kramer et al. 2004). These studies show that C I and CO emission trace each other well, independent of the type of heating environment. Since they share similar critical densities, $n_{\rm cr} \sim 10^3\,{\rm cm}^{-3}$, this suggests that the C I($^3P_1 \rightarrow {}^3P_0$) and ^{12}CO($J = 1 \rightarrow 0$) transitions arise from the same gas volume and have similar excitation temperatures (Ikeda et al. 2002). In addition, several studies have found excellent agreement between C I and CO derived H_2 masses in local ultraluminous infrared galaxies (ULIRGs; e.g. Gerin & Phillips 1998; Papadopoulos & Greve 2004).

Despite improved atmospheric observing conditions at the redshifted ($z > 2$) C I frequencies, observations of distant, faint sources are particularly difficult; neutral carbon has only been confirmed previously in four other high-redshift sources, three at $z \sim 2.5$ (Weiss et al. 2003, 2005) and one $z = 4.12$ quasi-stellar object (QSO; Pety et al. 2004). While it is challenging to detect, C I is a cooling line and therefore is important in understanding the composition of a galaxy's dense interstellar medium (ISM). In high-redshift sources, detection of C I indicates that the ISM has condensed and become significantly enriched while the Universe was still very young.

Here we report on the search for the upper fine structure line of neutral carbon, C I($^3P_2 \rightarrow {}^3P_1$), as well as the ^{12}CO($J = 7 \rightarrow 6$) line, towards two of the highest redshift and most luminous submillimetre galaxies (SMGs), GN 20 [$z = 4.055$, SMM J123711.9+622212, identified in Pope et al. (2006), whose redshift was accurately measured in Daddi et al. (2009), hereafter referred to as D09] and GN 20.2 [$z = 4.051$, SMM J123708.8+622202, also detected in ^{12}CO($J = 4 \rightarrow 3$) in D09; originally from the catalogue of Chapman et al. (2001)]. GN 20 ($S_{850} = 20.3$ mJy) and GN 20.2 ($S_{850} = 9.9$ mJy) are two of the brightest SMGs in Great Observatories Origin Deep Survey-North (GOODS-N; see also Pope 2007). Both of their rest-frame ultraviolet spectra lack any emission features (D09) and are similar to the UV spectra of many other $z \sim 2.5$ SMGs (Chapman et al. 2005). The absence of AGN characteristics in optical spectra suggests that the gas is mainly heated by star formation. Pope et al. (2006) have also shown that GN 20 has a very similar spectral energy distribution (SED) and mid-infrared (IR) spectral properties to other SMGs, as are its X-ray luminosity and photon index (cf. Alexander et al. 2005).

In addition to our interferometric millimetre observations from the Plateau de Bure Interferometer (PdBI), we present high-resolution radio maps of both galaxies at 1.4 GHz from MERLIN+VLA (Multi-Element Radio Linked Interferometer Network+Very Large Array) to further characterize these bright SMGs. We organize the paper as follows: observations are described in Section 2; results are discussed in Section 3 and our discussion of the implications on high-redshift SMG enrichment is given in Section 4. Throughout, we use a Λ cold dark matter (ΛCDM) cosmology with $H_0 = 71\,{\rm km\,s^{-1}\,Mpc^{-1}}$ and $\Omega_{\rm m} = 0.27$ (Hinshaw et al. 2009).

2 OBSERVATIONS

2.1 Molecular line observations

Observations were carried out with the IRAM PdBI through 2008 August, with a five-dish D-configuration (i.e. compact). We used the 2-mm receivers tuned to 159.873 GHz, mid-way between the expected redshifted frequencies of the C I($^3P_2 \rightarrow {}^3P_1$)($\nu_{\rm rest} = 809.342$ GHz) and ^{12}CO($J = 7 \rightarrow 6$) ($\nu_{\rm rest} = 806.651$ GHz) transitions for GN 20 at $z = 4.055$ and GN 20.2 at $z = 4.051$. The pointing centre was closer to GN 20 than to GN 20.2; since they are both off phase centre, their fluxes require primary beam attenuation correction factors of 1.11 (GN 20) and 2.62 (GN 20.2). This observation was made possible because of the redshift measurement from the ^{12}CO($J = 4 \rightarrow 3$) D09 observation. The synthesized beam size at 160 GHz is ≈3 arcsec. Calibration was obtained every 12 min using the standard hot/cold-load absorber measurements. The source 3C 454.3 was used for absolute flux calibration. The antenna gain was found to be consistent with the standard value of 29 Jy K^{-1} at 160 GHz. We estimate the flux density scale to be accurate to about ±15 per cent.

Data were recorded using both polarizations overlapping, covering a 900-MHz bandwidth. The total on-source integration time was 8 h. The data were processed using the GILDAS packages CLIC and MAPPING and analysed with our own IDL-based routines. The extracted data cube (two sky coordinate axes and one spectral axis) has an rms noise of 0.6 mJy. For clarity of presentation, we have regridded the data to a velocity resolution of ∼37 km s^{-1} (20 MHz). No obvious ($>5\sigma$) emission lines are seen in the data; however, the next section statistically tests for the presence of FIR continuum and CO and C I emission lines.

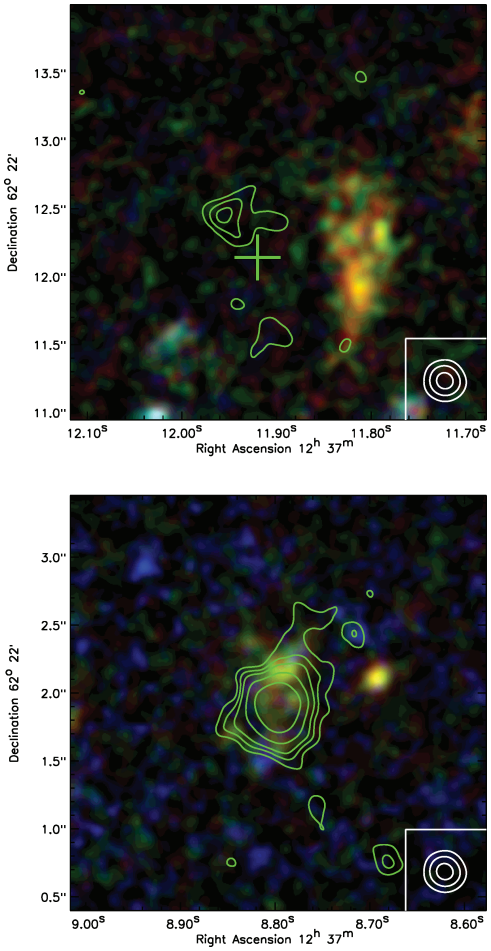

Figure 1. MERLIN+VLA radio contour overlay on *HST*/ACS *BVi* colour images of GN 20 and GN 20.2. The field sizes are 3 × 3 arcsec^2 and the MERLIN beam size is 0.3 arcsec (outer contour of corner inset is the FWHM of the beam). The levels of the radio contours are drawn at 3, 4, 5, 7 and 10σ; the rms noise in the MERLIN+VLA images is 2.9 and 4.6 μJy for GN 20 and GN 20.2, respectively. The centre of the SMA continuum emission analysed by Iono et al. (2006) and Younger et al. (2008) is marked by the green cross on the GN 20 map. The emission centroid for GN 20 in the mid-IR [*Spitzer* IRAC/MIPS (Infrared Array Camera/Multiband Imaging Photometer for *Spitzer*)] is consistent with the radio and FIR continuum position. The FIR–optical offset for GN 20 is significant at the 3σ level.

2.2 MERLIN+VLA radio imaging

High-resolution observations from the MERLIN (Thomasson 1986) were obtained for these sources as described in Muxlow et al. (2005), with an rms noise of ∼5 μJy beam^{-1}. While GN 20 or GN 20.2 were not imaged directly in Muxlow et al. (2005), the source is within the sensitive region of the data (Lovell Telescope primary beam). A combined MERLIN+VLA map was then constructed, with a sensitivity of 3–4 μJy beam^{-1} and high positional accuracy (tens of mas). In Fig. 1, we show MERLIN radio contours on top of the *Hubble Space Telescope* (*HST*) *BVi* tricolour images (Giavalisco et al. 2004).[1] The field size is 3 × 3 arcsec^2 and the restoring beam size is 0.3 arcsec. We measure the centre of MERLIN+VLA radio emission as 12:37:11.96, +62:22:12.4 for GN 20 and 12:37:08.80, +62:22:01.9 for GN 20.2.

[1] Based on observations made with the NASA/ESA *HST*, and obtained from the Hubble Legacy Archive, which is a collaboration among the Space Telescope Science Institute (STScI/NASA), the Space Telescope European Coordinating Facility (STECF/ESA) and the Canadian Astronomy Data Centre (CADC/NRC/CSA).

Table 1. Observed and derived properties of GN 20 and GN 20.2.

	GN 20	GN 20.2
$RA_{MERLIN+VLA}$ (J2000)	12:37:11.96	12:37:08.80
$Dec._{MERLIN+VLA}$ (J2000)	+62:22:12.4	+62:22:01.9
RA_{160} (J2000)	12:37:11.89	...
$Dec._{160}$ (J2000)	+62:22:12.4	...
$S_{1.4}{}^a$ (μJy)	73.8 ± 12.8	170.0 ± 12.8
$S_{3\,mm}{}^a$ (mJy)	0.33	<0.2
$S_{1.2\,mm}{}^a$ (mJy)	9.3	<2.7
$S_{1.1\,mm}{}^a$ (mJy)	11.5	...
$S_{850}{}^a$ (mJy)	20.3	9.9
$R_{1/2}$ MERLIN+VLA (arcsec)	0.38 ± 0.15	0.30
β	1.4 (derived)	1.5 (fixed)
L_{FIR} ($L_\odot$)	1.0×10^{13}	5.0×10^{12}
T_{dust} (K)	30 ± 4	30 ± 12
$z_{CO[4-3]}{}^b$	4.055 ± 0.001	4.051 ± 0.003
$I_{CO[4-3]}{}^b$ (Jy km s^{-1})	1.5 ± 0.2	0.9 ± 0.3
$L'_{CO[4-3]}{}^b$ (K km s^{-1} pc^2)	6.2×10^{10}	3.7×10^{10}
$M_{H_2}{}^{b,c}$ ($M_\odot$)	5.0×10^{10}	3.0×10^{10}
S_{160} continuum (mJy)	1.9 ± 0.2	0.5 ± 0.3
$I_{CO[7-6]} = I_{C\,I}$ (Jy km s^{-1})^d	<1.2	<1.9
$L'_{CO[7-6]} = L'_{C\,I}$ (K km s^{-1} pc^2)	$<1.6 \times 10^{10}$	$<2.5 \times 10^{10}$
M_{H_2} (from CO[7−6]) ($M_\odot$)	$<1.3 \times 10^{10}$	$<2.0 \times 10^{11}$
$M_{C\,I}/T_{ex}$ ($M_\odot$)	$<5.4 \times 10^6$	$<6.8 \times 10^6$
X[C I]/X[H$_2$]	$<1.8 \times 10^{-5}$	$<3.8 \times 10^{-5}$

Notes. We fit modified blackbodies to the FIR continuum flux densities (see Section 3.1) to derive dust temperature and L_{FIR} . β is reliably constrained to 1.4 for GN 20 and fixed to 1.5 for GN 20.2.

[a] Observed continuum flux densities from the literature at 850 μm (Pope et al. 2006), 1.1 mm (Perera et al. 2008), 1.2 mm (Greve et al. 2008) and 3 mm (D09). Upper limits for GN 20.2 are 2σ. The radio flux ($S_{1.4}$) is measured at 1.4 GHz from VLA.

[b] Observed properties from D09, given here for comparison.

[c] Derived from the measured D09 CO[4−3] line strength. D09 assumes a constant brightness temperature between ^{12}CO($J = 1 \rightarrow 0$) and ^{12}CO($J = 4 \rightarrow 3$) to derive M_{H_2}, but here we assume that $L'_{CO[4-3]}/L'_{CO[1-0]} = 8/16$ (cf. Weiss et al. 2007) and $L'_{CO[7-6]}/L'_{CO[1-0]} = 8/49$ (cf. Weiss et al. 2007). We also assume a conversion factor $X = M_{H_2}/L'_{CO} = 0.8\,M_\odot$ (K km s^{-1} pc^2)$^{-1}$ (cf. Downes & Solomon 1998).

[d] Line intensity limits are 2σ. In this data, both I_{CO} and $I_{C\,I}$ limits are equal since the noise measurement in each frequency range is equal, as are the assumed linewidths (700 km s^{-1}).

3 RESULTS

3.1 The continuum contribution at 1.88 mm

Interpreting the detectability and significance of emission lines in the millimetre requires an estimation of the expected continuum contribution at the wavelength of observations (160 GHz, which is a wavelength of ∼1.88 mm). Independent of our PdBI observations, we estimate the continuum flux at 1.88 mm by fitting modified-blackbody SEDs to the galaxies' FIR flux measurements. The continuum flux densities for GN 20 and GN 20.2 are given in Table 1. We fixed the emissivities of the galaxies to $\beta = 1.4$ for GN 20 (see Pope 2007) and $\beta = 1.5$ for GN 20.2 is common practice for galaxies in which β is not well constrained, although we note that letting β vary has a minimal effect, <10 per cent, on the continuum flux. With these SED constraints we measure the dust temperatures and

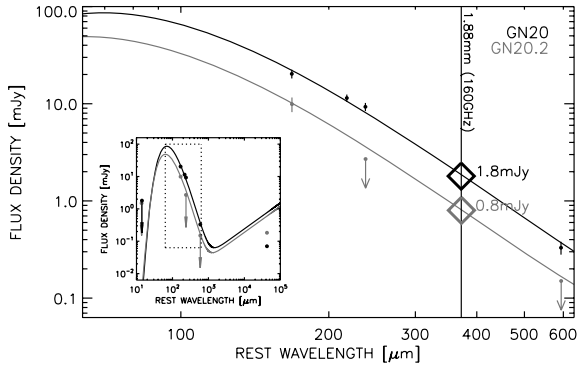

Figure 2. The SED fits to the FIR measured photometry of GN 20 (black) and GN 20.2 (grey). The inferred continuum flux densities at 1.88 mm are shown as large diamonds: 1.8 ± 0.4 mJy for GN 20 and 0.8 ± 0.4 mJy for GN 20.2. Their full SEDs from 10 μm near-IR to 10-cm radio (rest wavelength) are shown in the inset; the area outlined in the dotted box is the zoomed-in region shown in the larger plot.

FIR luminosities that are given in Table 1. The SED fits to both galaxies may be seen in Fig. 2. From these fits we infer that the 1.88-mm flux generated by FIR continuum should be 1.8 ± 0.4 and 0.8 ± 0.4 mJy for GN 20 and GN 20.2, respectively.

Having inferred the expected continuum level we must now *measure* the continuum from the 160-GHz PdBI observations. A one-dimensional (1D) spectrum for each object is first extracted at the peak integrated flux position, shown in Fig. 3. If we ignore the possible presence of emission lines, the average flux over the whole bandwidth is 1.9 ± 0.2 mJy for GN 20 and 0.5 ± 0.3 mJy for GN 20.2. The latter is consistent with the expected continuum flux, 0.8 ± 0.4 mJy, for GN 20.2, therefore, we conclude that neither C I($^3P_2 \rightarrow {}^3P_1$) nor ^{12}CO($J = 7 \rightarrow 6$) is detected in GN 20.2. The GN 20 average flux is consistent with the expected continuum level, 1.8 mJy, but since there is a large uncertainty in the expected flux at 1.88 mm, it needs to be further examined to see if the flux excess is due to the partial detection of C I and CO lines.

3.2 Placing limits on C I($^3P_2 \rightarrow {}^3P_1$) and ^{12}CO($J = 7 \rightarrow 6$)

Fig. 3 shows extracted 1D spectra alongside integrated channel maps for GN 20 and GN 20.2. The maps are centred on each galaxy's VLA radio position, and the 1D spectra are extracted at the point of peak integrated flux for GN 20 and at the VLA centroid for GN 20.2. Our observations have a ∼0.6 mJy rms noise near GN 20 and 1.6 mJy rms noise near GN 20.2 across the entire 900-MHz bandwidth.

To measure the continuum without allowing contamination from possible line emission, we must extract the portion of the GN 20 spectrum where line emission is anticipated. We use the measured D09 redshift and linewidth of ^{12}CO($J = 4 \rightarrow 3$) ($z = 4.055$ and $\Delta v \sim 700\,\mathrm{km\,s^{-1}}$) as an a priori condition and we apply them to both ^{12}CO($J = 7 \rightarrow 6$) and C I($^3P_2 \rightarrow {}^3P_1$) lines. Unfortunately, the narrow bandwidth limits the 'non-line' spectral portion to a small number of channels, specifically those with frequencies $159.75 < \nu_{\rm obs} < 159.95$ GHz or $\nu_{\rm obs} > 160.25$ GHz. We measure the continuum flux density in this spectral region to be S_{160}(GN 20) = 1.4 ± 0.3 mJy. This suggests that a flux excess *does* exist around the expected lines, from $159.95 < \nu_{\rm obs} < 160.25$ GHz (the C I line region) and at $\nu_{\rm obs} < 159.75$ GHz (the CO line region). To test the

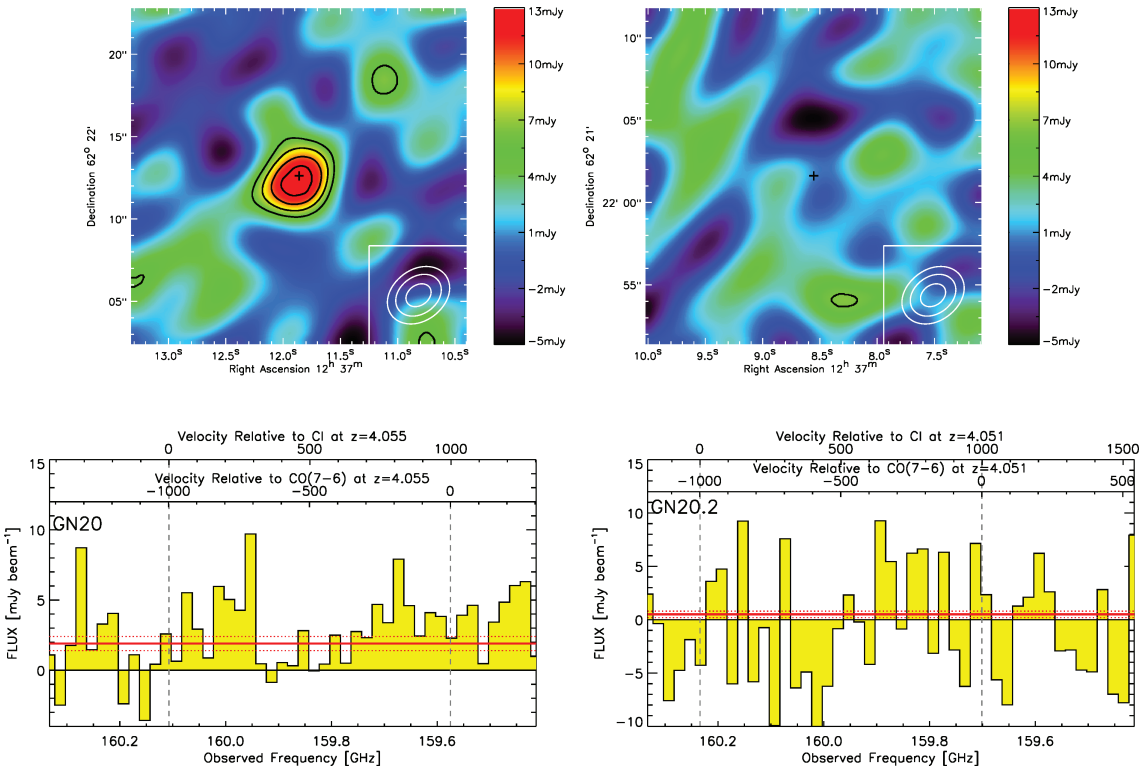

Figure 3. The 160-GHz maps and spectra for GN 20 (left) and GN 20.2 (right). The 20 × 20 arcsec^2 maps are integrated over the whole bandwidth; 4, 5, 6 and 7σ contours are overplotted (the detection of GN 20 is 8σ). The ∼3-arcsec beam shape is shown as a lower right insert in each map. The 20-MHz spectra are extracted at the peak flux position of GN 20 and at the VLA centroid position for GN 20.2. The average flux, or continuum estimation in the absence of line emission, is shown as a horizontal red line bounded by 1σ uncertainties (red dotted lines). The expected frequency centres of the C I and CO emission lines (based on the D09 redshift) are marked by dashed grey vertical lines.

significance of these excesses, we measure the mean flux density in each region and compare it to the 'non-line' flux. The average flux density is 1.6 ± 0.3 mJy in the C I line region and 2.5 ± 0.4 mJy in the CO region. Both excesses are of low significance ($<2\sigma$); thus, we conclude that neither ^{12}CO($J = 7 \rightarrow 6$) nor C I($^3P_2 \rightarrow {}^3P_1$) is detected in GN 20.

With no significant detection of CO or C I lines, we attribute all flux across the band to the FIR continuum, therefore, the measured continuum flux densities are 1.9 ± 0.2 mJy for GN 20 and 0.5 ± 0.3 mJy for GN 20.2. The latter is consistent with no detected continuum. The former continuum measurement for GN 20 is significant at the 8σ level. Although some flux from the emission lines might contribute to the flux density measurement of the continuum, we have not accounted for this additional uncertainty in our measurement.

We derive 2σ upper limits to C I and CO line intensities assuming the redshift and linewidth given by D09. For GN 20, we measure $I_{\rm C\,I} \approx I_{\rm CO} < 1.2$ Jy km s^{-1} (both limits are equal since the assumed linewidths and the noise measurements in each frequency range are equal). For GN 20.2, we measure $I_{\rm C\,I} \approx <1.9$ Jy km s^{-1}. The corresponding limits to line luminosity are given in Table 1.

3.3 CO excitation and brightness temperature

For interpreting CO line intensities, the assumption of constant brightness temperature has been widely taken a priori in the past due to lack of relevant data. However, many recent observations of multiple CO transitions in high-redshift sources have shown it to be an unwarranted assumption (Dannerbauer et al. 2009). Although detailed radiative transfer models demonstrate that the ^{12}CO($J = 1 \rightarrow 0$) and ^{12}CO($J = 3 \rightarrow 2$) transitions are near thermal equilibrium (i.e. $L'_{\rm CO(1-0)} \approx L'_{\rm CO(3-2)}$) for the three $z \sim 2.5$ sources studied (Weiss et al. 2005), there are several AGN-dominated galaxies which do not have constant brightness temperature for high-J transitions (e.g. FSC 10214+4724, APM 08279+5255 and the Cloverleaf quasar). Here we adopt the brightness temperature conversions for SMGs observed by Weiss et al. (2007), see their fig. 3; explicitly, we assume flux density ratios of $S_{\rm CO[4-3]}/S_{\rm CO[1-0]} = 10.0 \pm 0.8$ and $S_{\rm CO[7-6]}/S_{\rm CO[1-0]} = 8 \pm 1$. This implies $L'_{\rm CO[7-6]}/L'_{\rm CO[1-0]} = 8/49$ and $L'_{\rm CO[7-6]}/L'_{\rm CO[4-3]} = 64/245$. Working backwards from the D09 ^{12}CO($J = 4 \rightarrow 3$) detection, this implies that ^{12}CO($J = 7 \rightarrow 6$) in GN 20 would have luminosity $\sim 1.6 \times 10^{10}$ K km s^{-1} pc^2. We measure a line luminosity limit of $<1.6 \times 10^{10}$ K km s^{-1} pc ^{2}. While there are large uncertainties in our brightness temperature conversion assumption, this measured result for GN 20 agrees with the estimated population of the higher J transitions according to other high-z SMGs. Our data for GN 20.2 are less constraining due to the greater noise; our limit on line luminosity is consistent with $L'_{\rm CO[7-6]} \approx 1.2 \times 10^{10}$ K km s^{-1} pc ^{2}, which is the expected luminosity extrapolated from the ^{12}CO($J = 4 \rightarrow 3$) detection.

3.4 Radio source sizes

We use high-resolution MERLIN+VLA radio maps to constrain the size of the 1.4-GHz emission, to better assess the contributions from AGN and starbursts. The measurements of angular size were made using AIPS software JMFIT, deconvolving the restoring beam before attempting to derive the fitted Gaussian size. Since the signal-to-noise ratio is quite low in GN 20, it is impossible to detect component extensions smaller than the width of the restoring beam. Fig. 1 shows the MERLIN+VLA 1.4-GHz radio maps as contours on top of *HST* Advanced Camera for Surveys (ACS) i-band imaging. We measure the angular full width at half-maximum (FWHM) of the GN 20 emission region to be 0.38 ± 0.15 arcsec, but it is only significant above the 0.3-arcsec beam size at the 2.4σ level, while the 0.5-arcsec radio–optical offset is significant at the 3σ level.

Iono et al. (2006) showed that the 850-μm Smithsonian Millimetre Array (SMA) position of GN 20 was significantly offset from the optical emission (0.8-arcsec offset also at the 3σ level). Younger et al. (2008) obtained higher resolution continuum imaging of GN 20 with the SMA and constrained the size to 0.60 ± 0.13 arcsec claiming it to be partially resolved. This is consistent with our MERLIN+VLA measured size of 0.38 ± 0.15 arcsec due to the large uncertainties on both measurements. Because GN 20 is not exceptionally bright in the radio (74 μJy), we cannot determine if its asymmetric, extended MERLIN+VLA morphology is significant; therefore, we cannot rule out that GN 20 might be a radio point source dominated by AGN activity.

The radio source size of GN 20.2 is measured to be entirely unresolved at <0.30 arcsec. Radio emission with $S_{1.4} > 100$ μJy at $z = 4.051$ constrained by $R_{1/2} < 0.30$ arcsec would have to emit at a super-Eddington rate if it were completely dominated by star formation (a calculation based on the theoretical maximum star formation density given regulation by the dust Eddington limit in dense starbursts: c.f. Elmegreen 1996; Thompson, Quataert & Murray 2005). For this reason, GN 20.2's radio emission is likely partially generated, if not dominated by an AGN at the galaxy's core.

4 DISCUSSION

4.1 Neutral carbon and H_2 mass

Using the formulae given in Weiss et al. (2003) for the upper fine structure line of neutral carbon C I($^3P_2 \rightarrow {}^3P_1$), we can derive the mass of neutral carbon via

$$M_{\rm C\,I} = C\, m_{\rm C\,I}\, \frac{8\pi k \nu_0^2}{hc^3 A_{10}}\, Q(T_{\rm ex})\, \frac{1}{5}\, {\rm e}^{-T_2/T_{\rm ex}}\, L'_{\rm C\,I(^3P_2 \rightarrow {}^3P_1)}\, ({\rm M}_\odot), \qquad (1)$$

where $Q(T_{\rm ex}) = 1 + 3\,{\rm e}^{-T_1/T_{\rm ex}} + 5\,{\rm e}^{-T_2/T_{\rm ex}}$ is the neutral carbon partition function.[2] In the equation above, $T_1 = 23.6$ K and $T_2 = 62.5$ K represent the energies above the ground state, $L'_{\rm C\,I}(^3P_2 \rightarrow {}^3P_1)$ is given in K km s^{-1} pc ^{2}, $m_{\rm C\,I}$ is the mass of a single carbon atom and C is the conversion between cm^2 and pc^2, 9.5×10^{36} cm^2/pc^2. This assumes both carbon lines are in local thermodynamical equilibrium (LTE) and that C I emission is optically thin. Inserting numerical values in equation (1) yields

$$M_{\rm C\,I} = 4.566 \times 10^{-4}\, Q(T_{\rm ex})\, \frac{1}{5}\, {\rm e}^{-62.5/T_{\rm ex}}\, L'_{\rm C\,I(^3P_2 \rightarrow {}^3P_1)}\, ({\rm M}_\odot). \qquad (2)$$

Determining $M_{\rm C\,I}$ definitively requires measurement of the excitation temperature, which can only be done by detecting both C I($^3P_1 \rightarrow {}^3P_0$) and C I($^3P_2 \rightarrow {}^3P_1$), the two C I fine-structure lines. If $T_{\rm ex}$ cannot be measured directly, it is often assumed to be equal to the characteristic dust temperature [although in the case of the Cloverleaf quasar, Weiss et al. (2003) showed that $T_{\rm ex} = 30$ K, significantly less than the dust temperature, 50 K]. As the excitation temperature is unknown for both GN 20 and GN 20.2, we assume that $T_{\rm ex} = T_{\rm dust}$, which is appropriate, since here we are only able to derive upper limits on carbon mass for both systems. If the excitation

[2] We note that the negative sign in the exponent of $1/5\,{\rm e}^{-T_2/T_{\rm ex}}$ was accidentally omitted from the text of Weiss et al. (2003, 2005).

temperature is less than the dust temperatures (like the Cloverleaf), the upper limits on carbon mass would decrease. Without accounting for the possible magnification proposed by Pope (2007), we derive upper limits on carbon mass of $5.4 \times 10^6\,M_\odot$ (GN 20) and $6.8 \times 10^6\,M_\odot$ (GN 20.2).

Table 1 also lists the limits on H_2 mass derived from the ^{12}CO($J = 7 \rightarrow 6$) line luminosity limits, assuming brightness temperature conversions from Weiss et al. (2007) (see their equation 5). We also assume the standard ULIRG conversion factor $X = M_{H_2}/L'_{CO} = 0.8\,M_\odot\ (K\,km\,s^{-1}\,pc^2)^{-1}$ (Downes & Solomon 1998). Both the GN 20 and GN 20.2 ^{12}CO($J = 7 \rightarrow 6$) derived H_2 mass limits are in agreement with the ^{12}CO($J = 4 \rightarrow 3$) derived H_2 mass.

4.2 C I abundance in the molecular gas reservoir

Neutral carbon abundance, which is independent of magnification and adopted cosmology, is estimated using the ratio of masses between C I and H_2 through $X[C\,I]/X[H_2] = M_{C\,I}/(6\,M_{H_2})$. We calculate a carbon abundance upper limit using the M_{H_2} value derived by D09. We find that $X[C\,I]/X[H_2] \lesssim 1.8 \times 10^{-5}$ for GN 20 and $X[C\,I]/X[H_2] \lesssim 3.8 \times 10^{-5}$ for GN 20.2. Both limits are consistent with the C I abundance in the Milky Way Galaxy, $X[C\,I]/X[H_2] = 2.2 \times 10^{-5}$ (Frerking et al. 1989), but are much lower than the measured carbon abundances of local starburst galaxies $\sim 1.5 \times 10^{-3}$ ($\sim$50 times the abundance of the Milky Way; e.g. Schilke et al. 1993; White et al. 1994). Israel & Baas (2001, 2003) find similar carbon abundances in local ULIRGs although they account for total carbon mass instead of C I alone. In comparison, the handful of carbon abundance measurements that have been made at high redshift average to $\sim 5 \pm 3 \times 10^{-5}$ (e.g. Pety et al. 2004; Weiss et al. 2005). This is consistent with both the Milky Way's abundance and the two limits we have derived for GN 20 and GN 20.2. We note that an abundance near (or exceeding) that of the Milky Way implies that the cold molecular gas in GN 20 or GN 20.2 would already be significantly enriched 1.6 Gyr after the big bang (a possibility that is not excluded by our limits). More observations of C I and CO in high-redshift galaxies and QSOs are needed to investigate possible C I abundance variations with redshift or variations between differently heated environments (star formation dominant versus AGN).

5 CONCLUSIONS

GN 20 has become one of the best-studied high-redshift starburst systems in the GOODS-N field, due to its high apparent infrared luminosity. Its diverse multiwavelength coverage has revealed very low apparent levels of AGN emission relative to its high star formation. Observations of GN 20 in molecular emission lines have allowed a characterization of the system's gas properties, from the strong detection of ^{12}CO($J = 4 \rightarrow 3$) of D09 to the non-detections of C I($^3P_2 \rightarrow {}^3P_1$) and ^{12}CO($J = 7 \rightarrow 6$) in this paper. We have also characterized the molecular gas of GN 20.2, a nearby SMG at $z = 4.051$.

Millimetre and submillimetre continuum observations suggest a continuum flux density at 160 GHz of $S_{160\,GHz} = 1.8$ mJy for GN 20 and 0.8 mJy for GN 20.2. We measure 1.9 ± 0.2 mJy continuum for GN 20 and 0.5 ± 0.3 mJy continuum emission from GN 20.2. The former is significant at the 8σ level while the latter is not statistically different from zero.

GN 20 and GN 20.2 are undetected in C I($^3P_2 \rightarrow {}^3P_1$) and ^{12}CO($J = 7 \rightarrow 6$) using observations from the IRAM-PdBI in the D-configuration at 160 GHz. Line intensity upper limits are given as $I_{CO[7-6]}(GN\,20) = I_{C\,I}(GN\,20) < 1.2\,Jy\,km\,s^{-1}$, and $I_{CO[7-6]}(GN\,20.2) = I_{C\,I}(GN\,20.2) < 1.9\,Jy\,km\,s^{-1}$.

High-resolution radio imaging from MERLIN+VLA shows that the radio emission of GN 20 is extended over 0.38 ± 0.15 arcsec (2.7 kpc). This size is consistent with the FIR continuum size measured by Iono et al. (2006) and Younger et al. (2008). In contrast, GN 20.2 is unresolved at $<$0.30 arcsec (2.0 kpc), suggesting that AGN emission may dominate its radio emission.

The conditions for metal enrichment of the ISM of GN 20 and GN 20.2 do not appear to differ greatly with other high-redshift sources or the Milky Way. However, local starburst galaxies have $\sim$50 times the carbon abundance of the high-z systems and the upper limits for GN 20 and GN 20.2.

Future observations from the Atacama Large Millimetre Array (ALMA) of cooling gas emission lines like C I($^3P_1 \rightarrow {}^3P_0$) and C I($^3P_2 \rightarrow {}^3P_1$) in high-redshift sources will significantly advance the understanding of the relationship between early star formation and metal enrichment. Although difficult (in the absence of a boost from gravitational lensing) to observe with current instruments as evidenced by the lack of detection in GN 20, one of the brightest known high-redshift SMGs, C I is an excellent tracer of cold molecular gas in galaxies. It may even provide useful constraints on gas content when undetected relative to CO, and may be used as a powerful diagnostic of galaxy evolution out to the highest observable redshifts, especially in the light of the next generation of mm and submm telescopes.

ACKNOWLEDGMENTS

Based on observations carried out with the IRAM Plateau de Bure Interferometer. IRAM is supported by INSU/CNRS (France), MPG (Germany) and IGN (Spain). We acknowledge the use of GILDAS software (http://www.iram.fr/IRAMFR/GILDAS). CMC thanks the Gates-Cambridge Trust and IS thanks STFC for support. ED gratefully acknowledges funding support from ANR-08-JCJC-0008.

REFERENCES

Alexander D. M., Bauer F. E., Chapman S. C., Smail I., Blain A. W., Brandt W. N., Ivison R. J., 2005, ApJ, 632, 736
Bertoldi F. et al., 2003, A&A, 409, L47
Chapman S. C., Richards E. A., Lewis G. F., Wilson G., Barger A. J., 2001, ApJ, 548, L147
Chapman S. C., Blain A. W., Smail I., Ivison R. J., 2005, ApJ, 622, 772
Chapman S. C. et al., 2008, ApJ, 689, 889
Coppin K. E. K. et al., 2008, MNRAS, 389, 45
Daddi E. et al., 2009, ApJ, 694, 1517 (D09)
Dannerbauer H., Daddi E., Riechers D. A., Walter F., Carilli C. L., Dickinson M., Elbaz D., Morrison G. E., 2009, ApJ, 698, L178
Downes D., Solomon P. M., 1998, ApJ, 507, 615
Elmegreen B. G., 1999, ApJ, 517, 103
Frayer D. T. et al., 1999, ApJ, 514, L13
Frerking M. A., Keene J., Blake G. A., Phillips T. G., 1989, ApJ, 344, 311
Gerin M., Phillips T. G., 1998, ApJ, 509, L17
Gerin M., Phillips T. G., 2000, ApJ, 537, 644
Giavalisco M. et al., 2004, ApJ, 600, L93
Greve T. R. et al., 2005, MNRAS, 359, 1165
Greve T. R., Pope A., Scott D., Ivison R. J., Borys C., Conselice C. J., Bertoldi F., 2008, MNRAS, 389, 1489
Hinshaw G. et al., 2009, ApJS, 180, 225
Ikeda M., Oka T., Tatematsu K., Sekimoto Y., Yamamoto S., 2002, ApJS, 139, 467
Iono D. et al., 2006, ApJ, 640, L1
Israel F. P., Baas F., 2001, A&A, 371, 433

Israel F. P., Baas F., 2002, A&A, 383, 82
Israel F. P., Baas F., 2003, A&A, 404, 495
Kramer C., Jakob H., Mookerjea B., Schneider N., Brüll M., Stutzki J., 2004, A&A, 424, 887
Muxlow T. W. B. et al., 2005, MNRAS, 358, 1159
Narayanan D., Cox T. J., Hayward C., Younger J. D., Hernquist L., 2009, MNRAS, in press (arXiv:0905.2184)
Neri R. et al., 2003, ApJ, 597, L113
Ojha R. et al., 2001, ApJ, 548, 253
Papadopoulos P. P., Greve T. R., 2004, ApJ, 615, L29
Perera T. A. et al., 2008, MNRAS, 391, 1227
Pety J., Beelen A., Cox P., Downes D., Omont A., Bertoldi F., Carilli C. L., 2004, A&A, 428, L21
Pope E. A., 2007, PhD thesis, Univ. British Columbia
Pope A. et al., 2006, MNRAS, 370, 1185
Schilke P., Carlstrom J. E., Keene J., Phillips T. G., 1993, ApJ, 417, L67
Schneider N., Simon R., Kramer C., Kraemer K., Stutzki J., Mookerjea B., 2003, A&A, 406, 915
Solomon P. M., Vanden Bout P. A., 2005, ARA&A, 43, 677
Stutzki J. et al., 1997, ApJ, 477, L33
Tacconi L. J. et al., 2006, ApJ, 640, 228
Tacconi L. J. et al., 2008, ApJ, 680, 246
Thomasson P., 1986, QJRAS, 27, 413
Thompson T. A., Quataert E., Murray N., 2005, ApJ, 630, 167
Walter F. et al., 2003, Nat, 424, 406
Weiss A., Henkel C., Downes D., Walter F., 2003, A&A, 409, L41
Weiss A., Downes D., Henkel C., Walter F., 2005, A&A, 429, L25
Weiss A., Downes D., Walter F., Henkel C., 2007, in Baker A. J., Glenn J., Harris A. I., Mangum J. G., Yun M. S., eds, ASP Conf. Ser. Vol. 375, From Z-Machines to ALMA: (Sub)Millimeter Spectroscopy of Galaxies. Astron. Soc. Pac., San Francisco, p. 25
White G. J., Ellison B., Claude S., Dent W. R. F., Matheson D. N., 1994, A&A, 284, L23
Younger J. D. et al., 2008, ApJ, 688, 59

This paper has been typeset from a TEX/LATEX file prepared by the author.